STUDIES OF COAL AND CHAR PROPERTIES

Leslie L. Isaacs
Chemical Engineering Department
The City College of the
City University of New York
New York, New York 10031

INTRODUCTION

A thermodynamic data base is required both for the understanding and the proper design of processes utilizing coal and coal products. Since it is impractical to acquire the necessary data for each process and for each individual coal, it is important to establish predictive correlations between the physical and chemical parameters of the materials and their thermodynamic properties.

Heat capacity data can be used to calculate the variation of the thermodynamic properties, H,S.G, etc. with temperature. Conventional correlations of the heat capacities rely on the additivity approach, namely, that the total heat capacity of a dry coal is a matter, and inorganics (1,2,3). The correlation is successful in the sense that heat load calculations within 20% are possible.

The method has serious shortcomings inasmuch as it does not take into account the thermal history of the chars, the variability of the char structure with the rank of the parent coal and the interactions between the organic and inorganic components of the coal and/or of the char. Factors which affect the heat capacity of coals are:

- o The rank and inorganic matter content of the coal;
- o The moisture content;
- o The aging history of the coal sample.

Factors which affect the heat capacity of chars are:

- o The rank and inorganic matter content of the parent coal;
- o The gaseous atmosphere present during pyrolysis;
- o The thermal history of the char.

The history of a char is determined by:

- o The pyrolysis temperature;
- o The rate at which the coal temperature is increased from ambient to pyrolysis temperature;
- o The residence time of the char at the pyrolysis temperature.

Available data (4,5,6,7,8,9) for chars and coals cover limited temperature ranges and the thermal histories and compositions of the char samples are often ill-defined or unavailable. Thus, it was not possible to derive a universal correlation for the heat capacitie, taking the listed factors into account.

In an attempt to establish a thermodynamic data base for coals and chars and to assess the relative importance and effect of the factors listed, on the heat capacity, extensive work was undertaken and is continuing at City College (10,11,12,13). In this presentation we will limit ourselves to the discussion of results on chars.

EXPERIMENTAL DETAILS

A suite of samples was prepared for experimental work in a systematic manner. Three coals of different rank and petrography were used as starting materials. These selected 'parents' were a North Dakota lignite, an Illinois No. 6 HVB sub-bituminous, and a Virginia HVA sub-bituminous coal. The carbon content of these coals range from 63 to 73 weight percent (dry basis). The coals were ground in a ball mill to finer than 250 mesh. Half of the coal grounds were demineralized using the acid wash procedure (14). The other half was used without further treatment.

The pyrolysis was done in an inert atmosphere, by sweeping the furnace with nitrogen gas (1-SCFM flow rate). The samples were heated to the pyrolysis temperature with a relatively slow heating rate of 5°C per minute. Both pyrolysis temperature and residence time at temperature were used as variables for establishing thermal histories for the chars. Pyrolysis temperatures used were 500°C, 700°C, 900° C and 1100°C. Residence times were 0.1, 1, 2, and 24 hours. The char and coal samples were characterized by composition, porosity, pore size distribution and X-ray diffraction.

Heat capacity data were collected between 75K and 300K in a cryostat which was modified in order to use the adiabatic shield technique of calorimetry (15,16). To eliminate the contributions of adsorbed water to the specific heat, the experimental samples were vacuum dried at 110°C prior to loading into the calorimeter. The calorimeter was kept constantly under vacuum during the experimental runs. Each specimen was measured at least twice in separate experimental runs. The accuracy and reproducibility of the calorimetric data, and the validity of the data reduction scheme

were checked by the measurement and the determination of the heat capacity of copper and graphite samples (17,18,19). The data is judged reliable to one percent accuracy in the temperature range of 75K to 220K.

In the 150K to 1000K range heat capacity data was collected using a Differential Scanning Calorimeter (DSC). The heat capacities were measured under an Argon atmosphere. The raw DSC data were converted into heat capacities by calibration of the instrument using a Sapphire heat capacity standard. The accuracy of the DSC data is estimated at 2 percent.

RESULTS; EFFECT OF INORGANIC PHASE

The generality of the additivity hypothesis for the heat capacity of the chars was tested by determining the heat capacities of chars prepared from untreated coals, i.e., including the inorganic matter, and from coals which have been demineralized. The experimental data are shown in Figures 1,2, and 3. It was found that for the chars prepared from Illinois and Virginia coals the total heat capacity could be expressed on a weight basis as:

$$C_s = (1-w)C_o + wC_a \qquad 1)$$

Where C_s, C_o and C_a are the heat capacities of the char, ash free organic matter and ash respectively and w is the weight fraction of ash in the char. The temperature dependence of C_a in the 75K to 300K range varies depending on the origin of the ash.

The preparation of lignite based char from untreated coal is complicated by the catalytic effect of the included inorganic matter on the pyrolysis reaction. Both the rate of pyrolysis and the structure of the char formed are affected by the presence of inorganic matter. Therefore, it is not surprising that the total heat capacity of a lignitic char does not follow the additivity hypothesis.

The contribution of the ash to the total heat capacity of the char is not trivial. On a weight basis the ash heat capacity at room temperature is about four times greater than the heat capacity of the corresponding ash free organic matter in the char.

EFFECT OF PYROLYSIS TEMPERATURE AND CHAR PARENTAGE

The dependence of the heat capacities on pyrolysis temperature and origin was examined by determination of the heat capacities of chars prepared at several pyrolysis temperatures from demineralized coals with one hour residence time at the pyrolysis temperatures. In order to compare the data on the different chars quantitatively, the measured heat capacities must be corrected for residual ash contributions and need to be converted from a per unit mass to a per mole (ash free) atom basis.

The heat capacities at a given temperature, of chars of identical thermal history, are not simply related to the rank of the parent coal. As seen in Figure 4 the lignite chars have the highest heat capacities and Virginia chars the lowest at low temperatures. However, this order is reversed at high temperatures.

In Figures 5,6, and 7 the dependence of the char heat capacities on pyrolysis temperature are shown. The behavior is again complex. On a unit mass basis the heat capacities for a char of a given parentage shows cross-overs with temperature. This phenomenon is especially pronounced for the chars originating from the higher ranked coals.

EFFECT OF RESIDENCE TIME AT PYROLYSIS TEMPERATURE

Demineralized Virginia chars prepared at 1100^{o}C were used to investigate the effect of residence time on the heat capacities. The volatile matter was effectively removed from the coal by the time the pyrolysis reactor reached the pyrolysis temperature. Thus, the only further changes that occur as a function of time are dehydrogenation and graphitization (structural ordering) of the char. The heat capacities of the chars decrease with increasing residence time up to 1 hour, then increase for a 24-hour char. We show this behavior as heat capacity isotherms in Figure 8. This is interpreted as indicating that equilibration to a final H/C ratio at the pyrolysis temperature is a fast process relative to the ordering of the char which must take place by solid phase diffusion.

CORRELATION OF THE CHAR HEAT CAPACITY WITH PHYSICAL PARAMETERS

The primary interest in this research was to find a correlation between the heat capacities and physical parameters that characterize the chars. The parameters should include, at least, the char composition and the thermal history of the chars.

The heat capacity of a solid is reasonably well-described by the Debye theory. One can invert the heat capacity C_v using the well-known relation:

$$C_v = 9R(T/\theta)^3 \int_0^{\theta/T} \frac{u^4 e^4 du}{(e^u-1)^2} \qquad 2)$$

To obtain the effective Debye temperature θ as a function of temperature T, the measured specific heat obtained at constant-pressure conditions can be used instead of the constant-volume specific heat C_v, called for by the theory, since for a solid the difference between C_p and C_v is within experimental error at least below 300K. Values of the integral in Equation 2 can be found in standard tables (20). We were able to correlate $\theta(T)$ for the chars with parentage, composition and pyrolysis temperature T_p (in ^oK).

To apply the Debye model to a char, the ordinary theory must be modified (21). Consider that the carbon and "other kinds" of atoms of the char are distributed randomly in the solid matrix. Since the chars consist of about 90% (or more) carbon atoms, only carbon-carbon and carbon-"other" atom interactions need be considered for calculation of the char vibrational frequency spectrum. If the char consisted of carbon atoms only, the spectrum would depend solely on the arrangement of the carbon atoms in the matrix. The orderliness of this arrangement depends on the pyrolysis temperature (and residence time). This suggests use of the pyrolysis temperature T_p, as a nondimensionalizing parameter to calculate θ as a dunction of a reduced temperature $T_r=T/T_p$. This allows us to compare the effective Debye temperatures for chars of the same parentage but different thermal histories.

The carbon-other atom interactions will modify the vibrational spectrum by the addition of singular vibrational modes which will add onto the spectrum in the form of Einstein-like terms. These terms should, to the lowest order, be proportional to the product of the carbon atom abundance and the "other" atom abundance.

The correlation which was found (12) to fit the suggested model, using data from 75K to 300K, is given by:

$$\theta(T_r) = \theta_o (T_r) \exp [I(T_r)/x(1-x)] \qquad 3)$$

where 1-x = the atomic fraction of carbon in the ash-free char,
$\theta_o(T_r)$ = a Debye temperature at a given value of T_r for a char consisting of carbon atoms alone;
$I(T_r)$ = an interaction parameter connecting the carbon to the "other" atoms;
θ_o and I were found by trial and error fitting of Equation 3 to the experimental data.

At the present time we are continuing the interpretive work to refine the correlation equation and to include into it the residence time dependence of the heat capacities.

REFERENCES

1. N.Y. Kirov, Br. Coal Util. Res. Assoc. Mon. Bull., 29, 33 (1965).
2. W. Eiserman, P. Johnson and W.L. Conger, Fuel Processing Technology, 3, 39 (1980).
3. D. Merrick, Fuel 62, 540 (1983).
4. E. Melchoir and H. Luther, Fuel 61, 1071 (1983).
5. R.P. Tye, A.O. Desjarlais and J.M. Singer, High Temperature - High Pressures, 13, 57 (1981).
6. V.I. Kasatochkin, K. Usenbaev, V.M. Zhadanov, K. Sabyraliev, M. Rasalbaev, and K. Zhumalieva, Dokl. Akad., Nauk, S.S.S.R., 216, 93 (1974).
7. Internal Report of the Thermodynamics Research Group, Bartlesville Energy Research Center, DOE, "Thermal Data on Gasifier Streams from Synthane Test; (1973).
8. P. Delhaes and Y. Hishiyama, Carbon, 8, 31 (1970).
9. K. Kamiya, S. Mrozowski and A.S. Vagh, Carbon, 10, 267 (1972).
10. W.Y. Wang, Ph.D. Thesis submitted to the Graduate Faculty of Engineering, The City University of New York (Sept. 1981).
11. L.L. Isaacs and W.Y. Wang, "The Specific Heats of Coals and Chars" in the Proceedings of The Governor's Conference on Expanding the Use of Coal in New York State (M.H. Tress, J.C. Dawson, eds.) pp. 379-384 (May 1981).
12. L.L. Isaacs and W.Y. Wang, "Evaluation and Correlation of Coal Char Thermodynamic Functions" in Chemical Engineering Thermodynamics, (S.A. Newman, Ed., Ann Arbor Science) pp. 451-459 (1982).

REFERENCES (cont.)

13. L.L. Isaacs and E. Fisher, Preprint of Paper, A.C.S., Div. of Fuel Chem. 28, #2, pg. 240 (1983).

14. W. Radmacher and P. Mohrhauer, Brennst. Chemie, 236 (1955); M. Bishop and D.L. Ward, Fuel, 37, 191 (1968).

15. L.L. Isaacs and R.L. Panosh, Argonne National Laboratories' Communication Article ANL-MS01270 (1970).

16. L.L. Isaacs, Symposium, Cryogenic Experimental Apparatus, AIChE 71st Annual Meeting)1978).

17. G.T. Furakawa, W.G. Shaba and M.L. Reilly, NSROS-NBS-18, U.S. GPO, Washington, DC (1968).

18. W. Desorbo and W.W. Tyler, J. Chem. Phys. 21, 1660 (1953).

19. L.L. Isaacs and W.Y. Wang, "Thermal Properties of POCO-AMX Graphite", Thermal Conductivity 17 (J.G. Hust, Ed., Plenum Publishing Corp.) pg. 55 (1983).

20. K.S. Pitzer, Quantum Chemistry (Prentice Hall) p. 502 (1959).

21. Review Articles:
    (a) I.M. Lifshitz, Nuovo Cimento, Suppl., 10, 716 (1956).
    (b) A.A. Maradudin, P. Mazur, E.W. Montroll and G.H. Weiss, Revs. Mod. Phys., 30, 175 (1968).
    (c) A.A. Maradudin, E.W. Montroll, G.H. Weiss, Theory of Lattice Dynamics in the Harmonic Approximation, in "Solid Stat Physics," Suppl. 3, Academic Press, New York, 1963.
    (d) W. Ludwig, "Ergebnisse der exakten Naturwissenschaften," Volume 35, Springer, Berlin, 1964.
    (e) A.A. Maradudin, in "Phonons and Phonon Interactions," edited by T.A. Bak, W.A. Benjamin, New York, 1964, p. 424.
    (f) A.A. Maradudin, Theoretical and Experimental Aspects of the Effects of Point Defects and Disorder on the Vibrations of Crystals, in "Solid State Physics," volume 18, Academic Press, New York, 1966, p. 274.
    (g) G. Leibfried, Lattice Dynamics of Point Defects in "Atomic and Electronic Structure of Metals," (J.J. Gilman and W.A. Tiller, eds., Amer. Soc. for Metals) pg. 207 (1967).

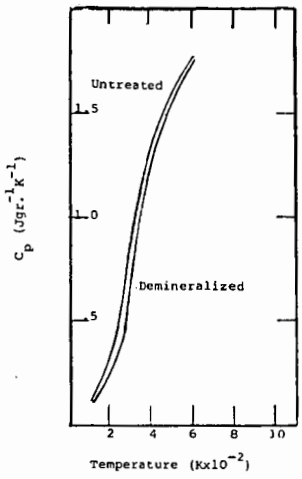

Figure 1. Illinois Char

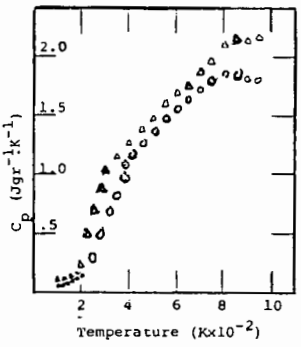

Figure 2. Virginia Chars
o Demineralized
Δ Untreated

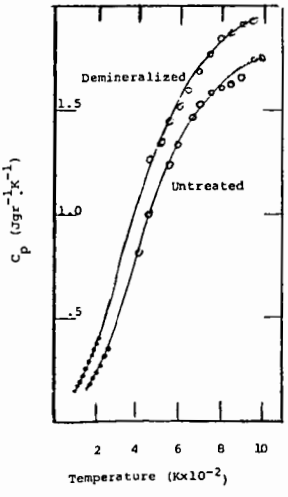

Figure 3. North Dakota Char

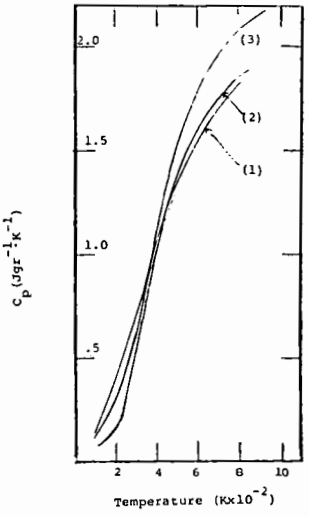

Figure 4. Demineralized Chars
(1) N. Dakota
(2) Virginia 700°C
(3) Illinois 1 Hour

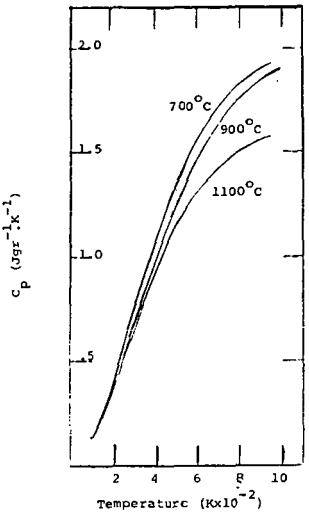

Figure 5. N. Dakota Chars

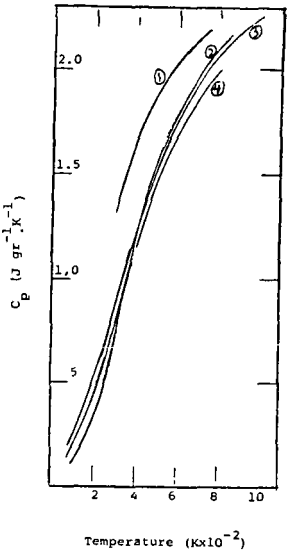

Figure 6. Illinois Chars
(1) 500°C (3) 900°C
(2) 700°C (4) 1100°C

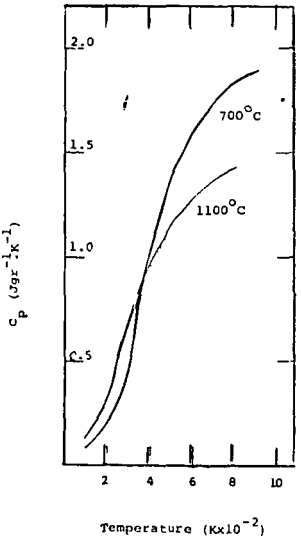

Figure 7. Virginia Chars

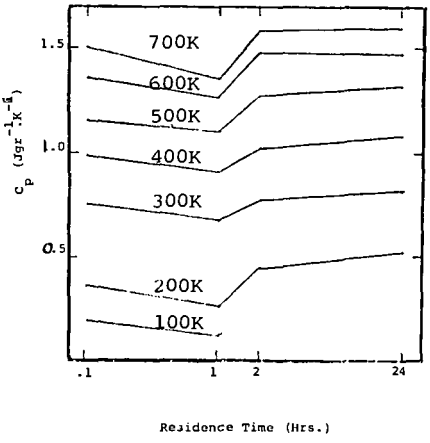

Figure 8. Virginia Chars

REMOVAL OF SYNTHETIC CRUDE NITROGENOUS COMPOUNDS USING WASTE MINERALS

BY

G. JEAN, M. POIRIER, and H. SAWATZKY

ENERGY RESEARCH LABORATORIES

CANMET, OTTAWA, CANADA, K1A 0G1

INTRODUCTION

Nitrogenous compounds in crude oils and petroleum products have been associated with several problems in processing operations and must be removed in the early stages of upgrading. With conventional technology this is done by severe hydrotreating which has several disadvantages: high capital cost investment, degradation of valuable material, and high operating cost due to energy and hydrogen consumption. A method allowing the separation of nitrogenous compounds from feedstocks would greatly reduce the costs of upgrading.

Several analytical procedures are known for the separation of nitrogenous compounds (1-7). These methods, however, are not feasible for large scale operation.

In this study waste minerals have been tested as low cost adsorbents. Since sulphide minerals are known as good adsorbents a series of sulphides was tested (5). We also tested brominated ilmenite in an attempt to take advantage of the complexing properties of titanium and iron (6,7).

EXPERIMENTAL

SULPHIDE MINERALS

The adsorption studies were conducted by liquid chromatographic methods. The feed was a solution of four or five nitrogenous model compounds dissolved in 50:50 heptane/toluene. Each compound contributed 25 ppm N to the solution. The adsorbents were natural waste minerals: pyrrhotite (FeS), pyrite (FeS_2), sphalerite (ZnS), and chalcopyrite ($FeCuS_2$).

The adsorbent (200 mesh) was dry-packed in a stainless steel column (60 cm long x 0.4 cm I.D.).

The solution of the nitrogen compounds was pumped into the column at 1 mL/min. Samples of 2 mL were collected and analyzed by gas chromatography using a Varian 6000 gas chromatograph and a Dexsil-300 packed column.

The area of the chromatographic peaks was used to calculate the percentage of each component present in the effluents. The calculations were made as follows:

$$\% \text{ Species } i = \frac{\text{area of peak } i \text{ in sample} \times 100}{\text{area of peak } i \text{ in feed}}$$

$$\% \text{ Total nitrogen} = \frac{\Sigma \text{ area of peak } i \text{ in sample} \times 100}{\Sigma \text{ area of peak } i \text{ in feed}}$$

Brominated Ilmenite

The ilmenite ore was taken from within 0.8 km of a point situated about 2.4 km southwest of St-Urbain and about 11.2 km north of the village of Baie St-Paul, Québec, on the north shore of the St-Lawrence River. It contained 39% TiO_2, 28% FeO and 19% Fe_2O_3. The ore was crushed to about 200 mesh and treated as follows:

In a 100-mL round bottom flash equipped with a reflux condenser, and containing 15-g of crushed ilmenite an excess of bromine (about 10 mL) was added. The mixture was heated to 58°C for 2 h, cooled, washed with 50-mL pentane to remove excess bromine. The treated ilmenite was filtered off and then washed again with pentane until the workings became colourless. The treated ilmenite was then dried with a stream of nitrogen, and used as adsorbent.

MODEL COMPOUND STUDY

A standard solution of 18 nitrogenous compounds in toluene was prepared. Its compositon is given in Table 1. This solution was pumped continuously at 0.5 mL/min into a 30 cm long x 0.4 cm I.D. column, packed with 20 g of treated ilmenite. Samples of 5-mL were collected and analyzed by gas chromatography using a 12.5 m long SE-30 capillary column.

RESULTS

The fate of the various nitrogenous compounds was monitored by analyzing the effluent by gas chromatography. A comparison of the results clearly shows that certain nitrogenous compounds have a greater affinity for the surface of the sulphides. Figure 1 shows the percentage of each species present in the effluent vs. the volume pumped into the column. These results show that three of the four compounds broke through the column after 5-mL compound was pumped. Tributylamine, however, was the only compound selectively removed. Thus the surface can differentiate between the various nitrogenous compounds. The same type of behaviour was observed for the other sulphide minerals.

Titanium is known to form complexes with various nitrogenous compounds (6,7). Ilmenite was treated with bromide in order to form $TiBr_x$ and $FeBr_x$ on the surface. Treated ilmenite was found to be a much better sorbent than untreated ilmenite. To better characterize the sorption properties of treated ilmenite a feed containing 18 model compounds was used. Figure 2 describes the fate of these 18 compounds during the run.

Compounds such as benzylamine and 2,2'-dipyridyl are extensively adsorbed and are still completely retained by the ilmenite after 150 mL has been pumped into the column. Other compounds such as carbazole are hardly adsorbed and elution occurs after 15 mL. The amount of benzylamine adsorbed is at least 20 times that of carbazole. Table 1 gives the order of elution of the 18 compounds. It is interesting to note that there seems to be a general correlation between the extent of adsorption and the basicity of the compound.

Another important feature observed in Fig. 2 is that some compounds are irreversibly adsorbed while others are reversibly adsorbed. Compounds such as indole are irreversibly adsorbed: in other words these compounds saturated the sites that were available to them and were not subsequently displaced. Conversely, compounds such as aniline are reversibly adsorbed. Their behaviour is typical of displacement chromatography where a compound is desorbed by another thus giving rise to a concentrated front that eventually elutes in the effluent. Figure 2 shows that these compounds elute in the effluent at a concentration of about three times that of the original feed. A rough mass balance indicates that these compounds are quantitatively desorbed and practically none is left on the column after the concentrated front has eluted.

DISCUSSION

The main conclusion in this study is that sulphide minerals have a very low adsorption capacity for nitrogenous compounds. These adsorbents, however, were found to be selective. For example, pyrrhotite adsorbs about 20 times more tributylamine than carbazole or trimethylpyrrole. The more basic compounds are usually more quantitatively adsorbed which suggests that these compounds are adsorbed on the Lewis and/or Bronsted acid sites. Therefore, increasing the surface acidity should increase the amount of nitrogenous compounds adsorbed.

Ilmenite was treated with bromide to form $TiBr_x$ and $FeBr_x$ on the surface. These salts are known as strong Lewis acids. The capacity of the treated ilmenite is much higher than that of the natural material.

The model compound study gives some insight into the adsorption mechanism. Indeed, the adsorptive properties of the 18 compounds differ depending on their nature. The compounds can be subdivided into four classes according to their adsorption behaviour as follows:

I	II	III	IV
carbazole	aniline	1,2,5-trimethylpyrrole	dibenzylamine
tetrahydrocarbazole	2-phenylpyridine	n-octylamine	1-phenethyl-piperidine
indole	3,4-benzacridine	n-decylamine	2,2'-dipyridyl
3-methylindole	quinoline	2-aminochrysene	benzylamine
phenothiazine	2-methylacridine		

In class 1 all compounds are pyrrolic with active protons on the nitrogen and are weakly acidic. Carbazole is hardly retained and the rest only slightly. Due to the absence of a concentrated elution front it appears that the adsorption is irreversible. In contrast, class II compounds, being weakly basic, are more quantitatively retained but are also displaced and elute as a concentrated front. Their behaviour is typical of displacement chromatography. Classes III and IV are definitely more basic and more quantitatively adsorbed. In class IV only benzylamine has broken through.

Since classes I and III, with the exception of the trimethylpyrrole, contain an active hydrogen, a possible explanation of these results is given below.

It is well known that titanium halides will react with primary and secondary amines to form a complex (6). Nitrogenous compounds with an active hydrogen can displace halides to give complexes $X_2Ti(NHR)_2$ or $X_3Ti(NR_2)$. Similar reactions are probably occurring at the surface of the treated ilmenite for titanium and iron salts.

$$MX_x + n(NH_2R) \rightarrow X_{x-n}M(NHR)_n + nHBR \qquad \text{Eq. 1}$$

or

$$MX_x + n(NHR_2) \rightarrow X_{x-n}M(NR_2)_n + nHBr \qquad \text{Eq. 2}$$

where M = Ti or Fe
X = halide
n = 1 or 2 depending on the nature of the amine
R = alkyl group

In this case adsorption is really a surface complexation. For purposes of this paper the term adsorption is used.

Contrary to class I, class II compounds were reversibly adsorbed. These compounds with the exception of aniline, do not have an active hydrogen on the nitrogen atom. This implies that the only mechanism of adsorption would be through the donation of the electron pair of the nitrogen to the Lewis centers. (Here, physical forces, interactions of the pi electrons with the surface, and hydrogen bond formation are neglected). The reaction can be illustrated as follows:

$$X_xM + :NR_3 \rightarrow X_xM:NR_3 \qquad \text{Eq. 3}$$

Delocalization of the lone pair of electrons over the ring decreases its availability for bonding. Since class II compounds are aromatics it is expected that they will form only weak bonds with the surface. This reaction is found to be reversible. The more basic compounds of classes III and IV probably displace compounds of class II according to the reaction:

$$X_xM:NR_3 + nNH_2R \rightarrow X_{x-n}M(NHR)_n + :NR_3 + nHBr \qquad \text{Eq. 4}$$

Class IV compounds have the highest affinity for the surface. These compounds are basic and will react with a great portion of the sites. 2,2[1] dipyridyl is particularly interesting. It does not have an active hydrogen on the nitrogen atom, but is known to be a strong ligand (8). It gives stronger complexes than ligands such as primary and secondary amines. It will react with the surface in a way similar to that described by Eq. 3.

The difference in adsorption capacity between the various classes can be explained in terms of their relative basicity. The surface is made of sites of various activity. The site distribution is expected to resemble a Boltzmann distribution where the highly active sites represent only a small fraction of the sites. The extent of adsorption of the nitrogenous compounds with the surface Lewis acids will depend on the availability of the lone pair of electrons on the nitrogen atom. Compounds of class I are not basic and will react only with the highly active sites. These represent only a small percentage of the sites which explains the low level of adsorption of class I compounds. Compounds of classesIII and IV are much more basic and will react with a much broader range of sites than those of class I and have a higher level of adsorption. Steric hindrance could also possibly play a role.

CONCLUSIONS

This study suggests that the adsorption of nitrogenous compounds on sulphide minerals and ilminite proceeds via an acid-base interaction. These adsorbents would successfully remove basic nitrogenous compounds, but not the acidic nitrogenous compounds. This implies that the effective capacity of the adsorbent will vary with the feed composition. This uncertainty would inhibit the use of such an adsorbent for routine use with feeds of changing composition such as petroleum feedstocks.

Therefore, the waste minerals investigated are not feasible adsorbentsfor industrial use. However, this study suggests a new approach to design an effective adsorbent. The ideal adsorbent would separate these compounds by a non-acid/base interaction which would allow both acid and basic nitrogenous compounds to be separated indiscriminantly. Such an adsorbent has been identified and the results will be pubished soon.

REFERENCES

1. Jewel, D.M., and Snyder, R.E., J. Chromatog., 38, 351 (1968)
2. Ford, C.D. et al. Anal. Chem., 53, 831 (1981)
3. Guerin, M.A. et al. Environ. Res., 23, 42 (1980)
4. Audeck, C.A., PREPRINTS, Div. of Petrol. Chem., ACS, 27, 998 (1982)
5. Jean, G.E., Ph.D. Thesis, University of Western Ontario (1983)
6. Cotton, F.A. and Wilkinson, G., Advanced Inorganic Chemistry, 3rd ed., Interscience Publishers, New York, (1972), p. 813
7. Ben Kovski, V.G. and Olzseva, M.D., Chem. Techn. of Fuel and Oil, 474 (1979)
8. Huhey, J.E., Inorganic Chemistry: principles of structures and reactivity, Harper and Row, Publishers, New York (1972)

TABLE 1

ORDER OF BREAKTHROUGH FOR MODEL COMPOUNDS

Curve No. on Fig. 2	Compound	Initial Concentration ppm	Volume at which 10% is reached (mL)	PKa*
1	Carbazole	25.24	1	
2	3-methylindole	26.74	20	
3	Phenothiazine	29.60	25	
4	Indole	29.37	31	
5	Tetrahydrocarbazole	27.70	30	
6	Aniline	30.12	45	4.63
7	2-phenylpyridine	24.26	45	
8	2-aminochrysene	13.90	45	
9	1,2,5-Trimethylpyrole	28.20	48	
10	3,4-benzacridine	7.85	51	
11	n-octylamine	32.62	55	10.65
12	n-decylamine	27.08	60	10.63
13	Quinoline	32.02	65	4.90
14	2-methylacridine	18.40	100	
15	Benzylamine	39.79	100	9.33
-	1-phenethylpiperidine	22.88	-	
-	2,2'-dipyridyl	55.58	-	
-	Dibenzylamine	26.48	-	

*CRC - Handbook of Chemistry and Physics, R.C. Weast Ed., CRC press 1976, 57th edition.

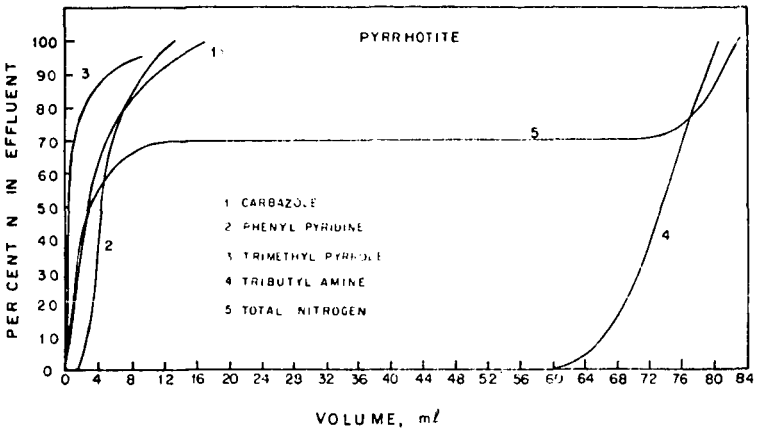

Fig. 1 - Adsorption of nitrogenous compounds on pyrrhotite

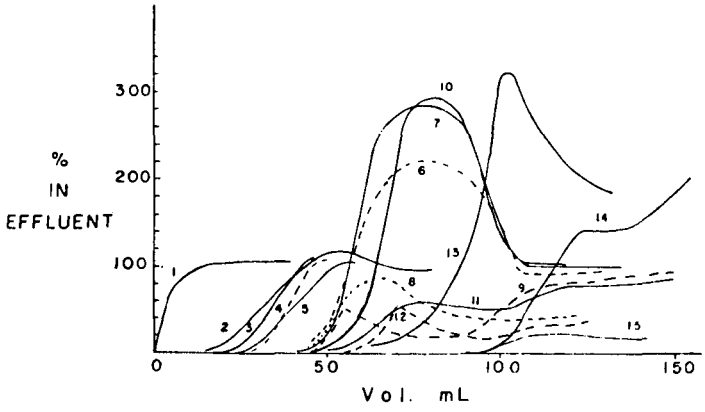

Fig. 2 - Breakthrough curves of individual compounds 1) carbazole; 2) 3-methylindole; 3) penothiazine; 4) indole; 5) tetrahydrocarbazole; 6) aniline; 7) 2-phenylpyridine; 8) 2-aminochrysene; 9) 1,2,5-trimethylpyrrole; 10) 3,4-benzacridine; 11) n-ocylamine; 12) n-decylamine; 13) quinoline; 14) 2-methylacridine; 15) benzylamine; not broken through: dibenzylamine; 1 phenethylpiperidine; 2,2[1] dipyridyl.

FT-IR DETERMINATION OF COAL AND SOOT PARTICLE TEMPERATURES DURING PYROLYSIS

Philip E. Best†, Robert M. Carangelo, and Peter R. Solomon, Advanced Fuel Research, Inc., 87 Church Street, East Hartford, CT 06108.

INTRODUCTION

The literature currently reports up to four orders of magnitude variation in the rate for coal pyrolysis at high temperature. The discussion of this problem with references to the literature is presented in (1,2). The wide variations appear to be caused by the inability to separate heat transfer from chemical kinetics. To resolve this issue, it is essential to measure particle temperatures in a pyrolyzing or combusting system. Several (two or more) color pyrometry systems have been developed for this purpose. A system which allows the measurement of single particle temperatures simultaneously with particle size and velocity was recently described by Tichenor et al. (3). The ability to measure temperatures of individual particles is important when there are temperature differences among particles. However, these systems have some disadvantages which limit their application. They employ wavelengths in the visible, which misses most of the emitted radiation. It is difficult to measure low temperatures (Tichenor et al. (3) estimate a 900 K limit for 10 micron particles) and to distinguish particle temperatures in the presence of soot or high temperature regions which can reflect radiation from the particle. Also, particle densities must be low, and it may sometimes be difficult to get a complete picture of a reacting system because low temperature particles will be overlooked.

The application of FT-IR emission and transmission spectroscopy is a good complement to the measurements in the visible, having advantages where the pyrometric techniques have disadvantages. It appears that contributions from soot and particulates can be separated by examining both the emission and transmission spectra and employing a knowledge of the soot's characteristic signature in the IR. Under conditions of uniform temperatures, particulate temperatures and soot densities can be determined. The FT-IR technique has advantages at low temperatures. At the temperatures of interest the emitted radiation has a maximum in the IR, providing good sensitivity. Also, because the measured spectrum covers the whole infrared range, the optical properties of the coal, char and soot (which vary in the infrared) can be measured and used to distinguish the nature of the particulates and the magnitude of reflected radiation. Finally, the technique can determine temperature for clouds of particles by comparing both the amplitude and shape of the emission and transmission spectra.

This paper discusses the application of the technique and preliminary results in a study of coal and acetylene pyrolysis.

EXPERIMENTAL

The emission of infrared light from, and transmission through, dispersed particles involves the processes of emission and absorption in the particle's interior, and reflection, diffraction and refraction at its surfaces. The infrared energy in these measurements can originate in the spectrometer, in the particles or from the hot experimental apparatus. To sort out these effects, as well as the influence of temperature, coal composition and morphology on the spectra, the studies described below have been carried out in a number of geometries.

Measurements In A Hot Cavity

Emission and transmission spectra were recorded in an entrained flow reactor (EFR) in which coal particles are fed into the furnace from a water cooled injector. In this geometry the coal "sees" hot furnace walls with the exception of the injector and the KBr windows that provide entrance and exit for the IR beam.

† permanent address: Department of Physics and Insitute of Material Science, University of Connecticut, Storrs, CT 06268

Transmission spectra are recorded in the normal manner, as the ratio of transmission with and without the sample in the beam. In this experiment, the radiation from the spectrometer is amplitude modulated, so radiation originating from within the furnace is not detected. In the sample area, the beam geometry is identical for the emission and transmission experiments. In the emission experiment the detection sensitivity is wavelength dependent. The overall detection efficiency is measured by recording the spectrum from a cavity radiator of known temperature. The cavity serves both to provide a path correction at each wavenumber, and as a reference for the calculation of the shape and amplitude of black-body radiators of other temperatures. The reported emission spectra are also corrected for background.

An example of an emission spectrum for lignite in the furnace is presented in Fig. 1a. For the conditions at which each emission spectrum was recorded a corresponding transmission measurement was made, as shown in Fig. 1b which presents (1-transmission). Except for the gas lines, these spectra show a monotonic variation with wavenumber in a manner which can be accounted for by diffraction theory (2). Since we want to compare emission from particles which fill only a fraction of the viewing area with that from the cavity which fills 100% of the viewing area, we have computed a "normalized emission", Fig. 1c, in which the emission is divided by (1-transmission). The detailed significance of this "normalized emission" will be considered later. For the present we will discuss this function for the case in which the coal particles are of such size and texture that each one effectively blocks 100% of the radiation incident on it. In addition, we work in a dilute particle regime, so that less than 20% of the total beam is blocked. The particles can be considered to act as individual scatterers. In this case (1-transmission) is a measure of the projected area of the coal particles, and represents the fraction of the beam blocked by the sample. It also represents the projected emitting surface area as a fraction of the beam area. If we divide an emission spectrum by the corresponding (1-transmission) we obtain the spectrum that would appear if the sample completely filled the entrance aperture. We call these "normalized emission" spectra. The normalized spectra from a sample of black-body particles at temperature T would agree in shape and amplitude with the black-body spectrum corresponding to temperature T and generated from the information in the reference source spectrum. A similar set of emission, transmission and "normalized emission" spectra is presented for soot (Fig. 2). For sufficiently small soot particles the normalized spectrum can be rigorously equated to a black-body curve at the soot temperature. An appropriate theoretical black-body curve is also presented in Figs. 1c and 2c. Indeed, the "normalized emission" is quite close to the theoretical black-body in both shape and amplitude.

An example of normalized emission data, obtained for a lignite injected at several positions above the optical port in the EFR, is presented in Fig. 3. The data illustrate some of the potential benefits as well as the caution required in the interpretation. The figure shows the normalized emission spectra compared to a theoretical black-body curve at the window height wall temperature. Figure 3a presents data for coal injected just above the port. The coal at this position is **cold.** But there is obviously radiation emerging from the optical port which was not there in the absence of the coal. This must be scattered radiation. As the coal's residence time increases between injection and observation, the spectrum gets closer to the spectrum for the wall. At 36 cm the coal's absorption spectrum is gone, and the spectrum amplitude and temperature is higher than that of the wall. In this case the coal is cooling after having been heated to a higher temperature in the upper part of the furnace. This measurement without any further information can be used to determine the distance required for the coal to reach the reactor temperature.

For later purposes we have also reported the normalized emission from KCl particles in the EFR (Fig.4).

Measurements In A Room Temperature Cavity

To allow separation of contributions from emission and scattering, a second geometry was used employing a tube furnace. In this experiment, the particles have been

heated in a high temperature tube prior to their coming into view of the IR beam. The turbulent environment of the tube convectively heats the coal particles very quickly ($>10^5$ K/sec). The only hot surface seen by the coal when it is in view is the overhead tube. Since the FT-IR spectrometer transmits only radiation which has its electric vector in the vertical plane, radiation from the tube scattered by one scattering event cannot be detected, in contrast to the case for the EFR experiment in which there ia substantial scattering of wall radiations.

Figure 5 presents "normalized emission" spectra taken at the exit of the tube reactor after sufficient residence time to bring the coal up to the tube temperature. Each spectrum is compared with a black-body curve at the measured gas temperature at the position of the optical focus. At temperatures below 650 K, (Fig. 5a and b), only the region below 1700 wavenumbers has sufficient emissivity (absorptivity) to emit much radiation. As discussed later, the emissivity, ϵ_ν, of the coal can be calculated from the data of Fig. 5 together with the extinction coefficient. We have calculated ϵ_ν from the data of Fig. 5d and used it to compute the fraction of radiation from a 1800 K environment that is absorbed by the coal. The results indicate an equivalent grey-body emissivity of 0.2. **Raw coal of pulverized coal size is, therefore, a poor emitter of radiation and consequently, is a poor absorber of radiation. It absorbs much less radiative energy than is usually computed assuming a grey-body with ϵ = 0.7 to 1.0.** This fact is important in computing the heating rate of the coal.

At temperatures of 750 K and 825 K the hydroxyl and aliphatic regions of the coal begin to emit (Figs. 5c and d). At 925 K, char condensation reactions are starting to produce a broad band emission as the char behaves more "graphitic"; this trend continues until, at 1200 K, the char is a grey-body with an emissivity between .7 and .8, similar to that of graphite.

Transmission And Reflection Measurements

Transmission measurements of coal in KBr pellets of coal films were recorded in a typical sample holder geometry for this experiment. The abaorbances of two coal filma of the same nominal thickness were measured. Figure 6a shows the spectrum of a uniform film of 1μm particles pressed into a KBr flat. The spectrum of Fig. 6b is for a film pressed at moderate pressure from a starting material of nominal 30μm diameter particles. Under an optical microscope the surface roughness of this latter film appeared comparable to that of an unpressed sample of the same coal. These spectra display the effect of morphology. The film made of ground (1μm) diameter particles has residual surface inhomogeneities of the order of the original particle size and can be expected to strongly scatter wavelengths in this region, with the scattering falling off aa ($1/\lambda^4$) towards longer wavelengths. In the region of 1800 cm^{-1} this 40μm thick film is moderately transparent. Extinction at longer wavelengths is due primarily to absorption, while at shorter wavelengths there is increased extinction due to scattering as well as absorption. For a film of similar thickness, but made of pressed 30μm diameter particles, (Fig. 6b) extinction over the long wavelength end of the spectrum is dramatically increased, showing qualitatively the dominance of scattering. The coal particles in our experiments have inhomogeneities more of the scale of the film of Fig. 6b than that of Fig. 6a: **scattering plays a significant part in the interaction of the particles with radiation.**

The specular reflection of coal was meaaured at an angle of incidence of 45° (Fig. 6c). This spectrum can be accounted for by standard theory using optical constants which lie within the range of published values (5). The reflection is small, (between 6 and 10%) and will be important only for rays which nearly graze the surface.

DISCUSSION

The scattering, absorption, transmission and emission of electromagnetic radiation from particles depend both on material properties in the form of the optical

constants, and on morphology, which can be represented by the scales of inhomogeneity relative to wavelength. The interaction of particles with the radiation field is characterized by efficiency factors, Q, which are the effective cross sections for scattering or absorption divided by the geometric cross section of the particles.

$$Q_{ext} = Q_s + Q_{abs} \tag{1}$$

where the subscripts stand for extinction, scattering and absorption, respectively (6). Q_s refers to radiation scattered out of the acceptance angle of the optics. Similarly, the other Q'_s are specific to our optical beam path. We will describe a simple model that semiquantitatively accounts for many features of the observed normalized emission spectra. The first feature of the model is due to the geometry of the experiment in the EFR. In this geometry, radiation from the transmission beam can scatter into almost a 360° solid angle of the furnace, while conversely, radiation from this almost 360° solid angle can scatter into the emisson beam. The beam-defining aperture is just smaller than the furnace wall opening. For particles within the focus volume, for each incident beam 1 scattered into direction 2, we can find a beam 1' from the furnace wall that is scattered through the same angle into the original beam direction 2' (Fig. 7). From this discussion the following statement can made about the relative scattering in emission and transmission experiments. If Q_s is the efficiency for scattering out of the beam path in a transmission experiment in this EFR, then

$$Q_s = Q's \tag{2}$$

where Q'_s is the efficiency for scattering wall radiation into the beam in an emission experiment, for particles within the focus volume. All the Q's and ε's that we subsequently discuss are wavenumber dependent but we have dropped the subscript, ν, for convenience.

If we observe the particle in an isothermal environment, then with the usual Kirchoff analysis, the radiation entering the optical aperture of the spectrometer would be

$$Q'_s \cdot BB(T) + \varepsilon \cdot BB(T) = BB(T) \tag{3}$$

when the transmission through the particle is zero and where ε is the particle emissivity into the spectrometer acceptance angle, compared to the black-body emissivity of unity and where BB(T) is the black-body spectrum corresponding to temperature T. As usual,

$$\varepsilon = Q_{abs} \tag{4}$$

where both parameters refer to radiation entering or leaving the particle in the cone defined by the spectrometer aperture.

With these definitions we describe the normalized emission results as

$$\frac{\text{("observed emission")}}{\text{(1-transmission)}} = \frac{N_p \cdot A_p \cdot \left[\varepsilon \cdot BB(T_p) + Q's \cdot BB(T_w)\right]}{N_p \cdot A_p \cdot (Q_{abs} + Q_s)}$$

$$= \frac{Q_{abs} \cdot BB(T_p) + Qs \cdot BB(T_w)}{Q_{abs} + Q_s} \tag{5}$$

where $BB(T_p)$ and $BB(T_w)$ are the black-body emission curves appropriate to the particle and EFR wall temperatures, respectively, N_p and A_p are the numbers of

particles in view, and their average geometrical cross-section, respectively. Equation 5 can be applied to explain the results of Figs. 1-5.

Case 1) If $Q_{abs} \approx 0$, as for KCl, the normalized emission should be equivalent in shape and amplitude to $BB(T_w)$, as is observed (Fig. 4).

Case 2) For soot particles of sufficiently small dimensions, the scattering is negligible (7). In that case the normalized emission (eq. 5) is given by $Q_{abs} \cdot BB(T_p) / Q_{abs} = BB(T_p)$. This predicts that the normalized emission from soot will be equal in amplitude and shape to the black-body curve corresponding to the soot temperature. This is indeed the case (Fig. 2). **For KCl and soot, as well as all subsequent cases, there are no adjustable parameters in the comparisons we make.**

Case 3) Another occasion in which a particularly simple result comes from this analysis is when the particle and wall temperatures are the same. Equation 5 shows that the normalized emission will be a good black-body curve, this time corresponding to the wall (and particle) temperature (Fig. 1).

The last cases to be considered are when non-black-body shape or amplitude is observed in the normalized emission (Figs. 3 and 5).

Case 4) Taking the case of the tube furnace first, and noting that there is no wall radiation to be scattered into the spectrometer in an emission measurement in that situation, the normalized emission is

$$\mathcal{E} \cdot BB(T_p)/(Q_{abs} + Q_s) \qquad (6)$$

For coal particles, the variation of the demoninator of eq. 5 with wavenumber is similar to that of Fig. 1b: $Q_{ext} = Q_{abs} + Q_s$ has a value between 1 and 2, which can be estimated from diffraction theory (2). Multiplying the normalized emission by Q_{ext}, and dividing by the black-body curve corresponding to the messured temperature, gives an experimental estimate of $\mathcal{E}$, the coal emissivity. As expected from eq. 4, maxima in the emission in the tube furnace spectra (Fig. 5) correspond to maxima in the absorbance spectrum of the coal (Fig. 6).

Case 5) The most difficult case is for particles in the EFR where contributions come from both emission and scattering. In this case one can select regions of the spectrum which still permit simplification. For regions where the coal absorbs strongly (eg. 1600 cm^{-1}), Qabs approaches unity for sufficiently large particles. Such regions of the spectrum can be used to determine the particle temperature.

CONCLUSIONS

Normalized FT-IR emission spectra appear to contain a considerable amount of information about the solid phases in pyrolyzing coal and gas systems. In this preliminary work we have deduced solid phase temperatures for a number of circumstances, demonstrated the ability to detect chemical change in high temperature reactions, and deduced a grey-body emissivity for coal. With improved evaluation of how the emissivity changes with pyrolyis, there are good prospects that the temperature determining capability of the method can be extended.

ACKNOWLEDGEMENTS

This work was supported by the U. S. Department of Energy, Morgantown Energy Technology Center under Contract No. DE-AC21-81FE05122, U.S. Department of Energy, Pittsburgh Energy Technology Center under Contract No. DE-AC22-82PC50254 and The National Science Foundation under Contract No. CPE-83-60666.

REFERENCES

1. Solomon, P.R., Hamblen, D.G., Carangelo, R.M., Markham, J.R., and DiTaranto, M.B., ACS Division of Fuel Chemistry Preprints 29, #2, p. 3 (1984).

2. Solomon, P.R. and Hamblen, D.G., Finding Order in Coal Pyrolysis Kinetics, Progress in Energy and Combustion Science, 9, 323 (1983).

3. Tichenor, D.A., Mitchell, R.E., Hencken, K.R. and Niksa, S., Simultaneous In-Situ Measurement of the Size, Temperature and Velocity of Particles in a Combustion Environment , presentation at the 20th Symposium (Int) Conference on Combustion, Aug. 12-17, 1984, University of Michigan, Ann Arbor Michigan.

4. Gumbrecht, R.O. and Sliepcevich, C.M., J. Phys. Chem. 57, 90 (1953).

5. Foster, P.J. and Howarth, C.R., Carbon, 6, 719, (1968).

6. van de Hulst, H.C., Light Scattering by Small Particles , Dover Publications, NY, (1981).

6. D'Alessio, A., Cavaliere, A. and Menna, P., **Soot in Combustion Systems**, Edited by J. Lahaye and G. Prado, Vol. 7, pg. 327, (Plenumn Press, NY), (1983).

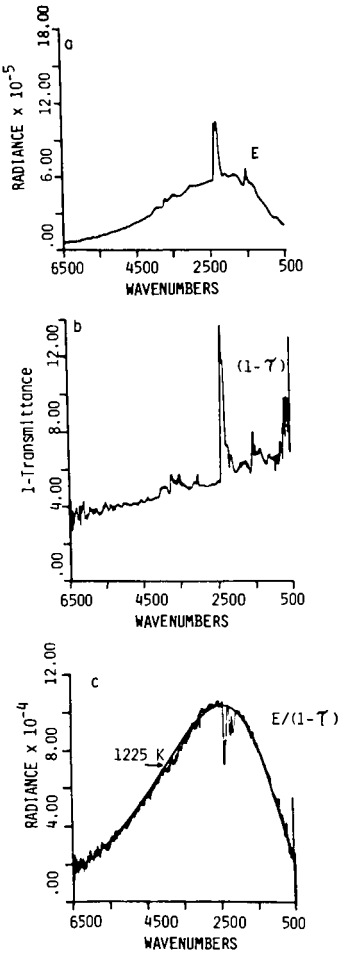

Figure 1. a) Emission, b) (1-transmission), and c) $E/(1-\tau)$, Curves for a Lignite (mesh size -300 +425) Injected into the Furnace at 36 cm above the Window. Furnace Wall Temperature at Window Height is 1170 K.

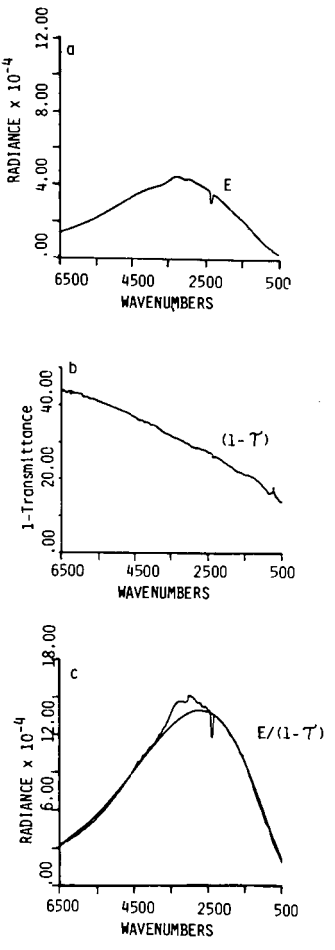

Figure 2. a) Emission, b) (1-transmission), and c) $E/(1-\tau)$, Curves for Soot formed by Acetylene Injected into a Furnace at a Height of 66 cm above the Window. Furnace Wall Temperature is 1250 K. Curve c is a Quantitative Black-body Curve Corresponding to a Temperature of 1350 K.

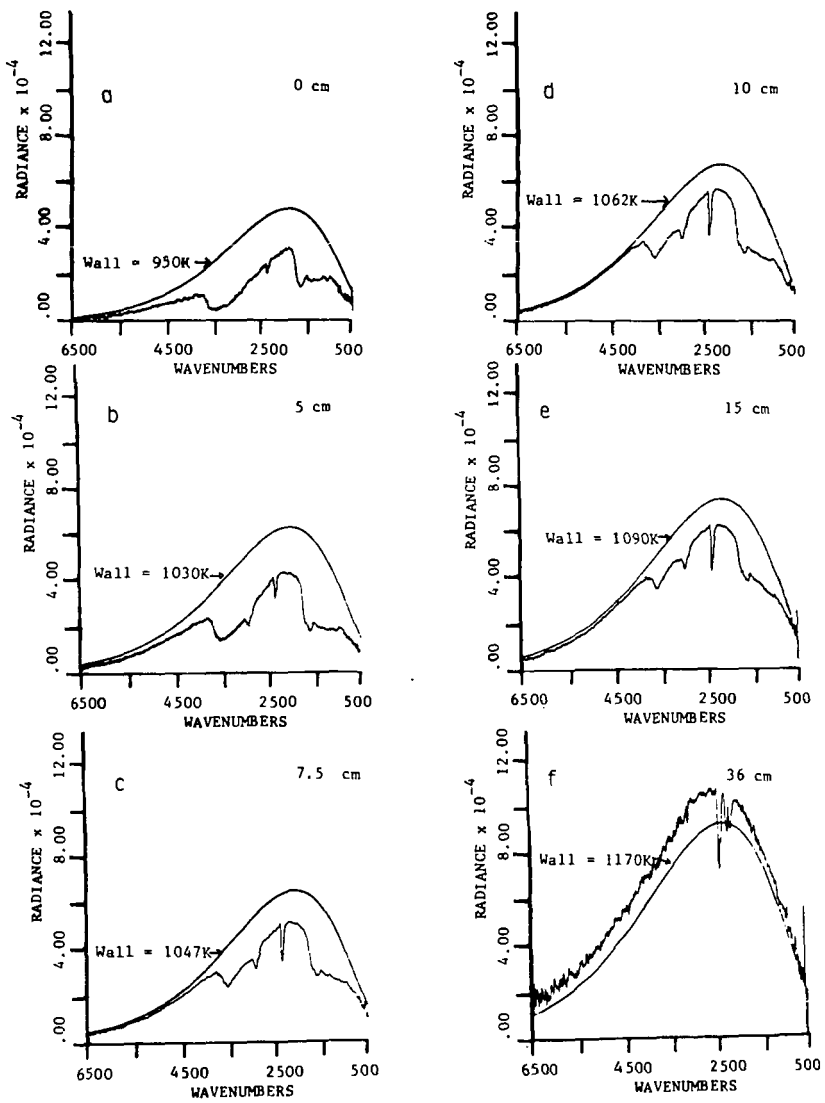

Figure 3. Series of E/(1-τ) Curves for Lignite Particles in the Furnace for Increasing Residence Time.

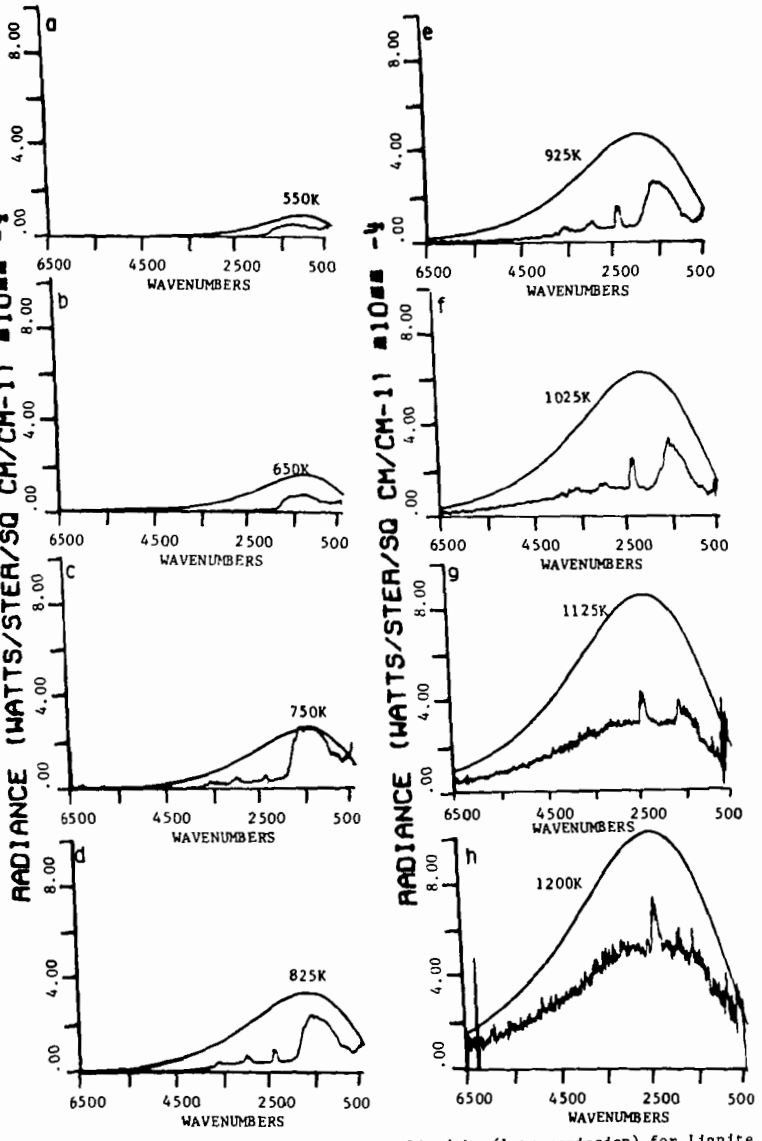

Figure 5. Series of Emission Normalized by (1-transmission) for Lignite Particles in the Tube Reactor for Increasing Temperature.

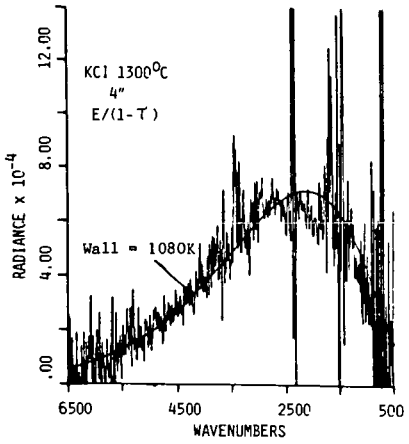

Figure 4. $E/(1-\tau)$ for Cold KCl Particles in a Hot Furnace. Furnace Wall Temperature is 1080 K. This Curve is a Quantitative Black-body Curve Corresponding to a Temperature of 1080 K.

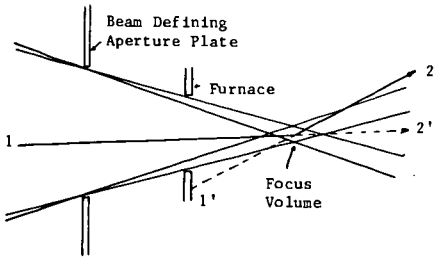

Figure 7. Configuration of Beam Defining Aperture and Furnace Wall in EFR.

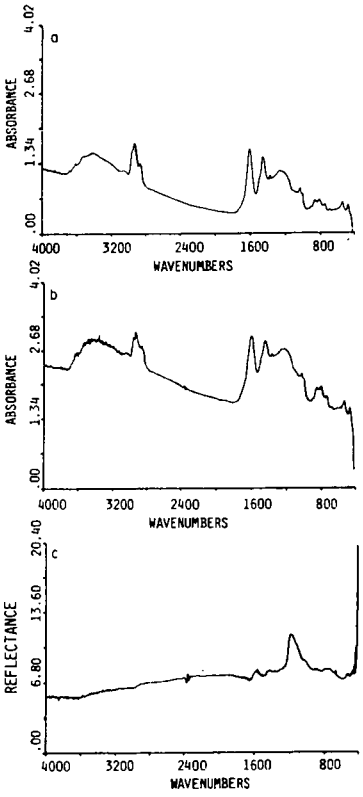

Figure 6. a) Spectrum of 40 μm Coal Film Pressed from 1 μm Diameter Particles, b) Spectrum of 40 μm Coal Film Pressed from 30 μm Particles, and c) Specular Reflection of a Coal Pellet Pressed from 1 μm Diameter Particles.

THE EFFECT OF OXIDATION OF COAL ON THE COMPOSITION OF LIQUEFACTION PRODUCTS

Muthu S. Sundaram* and Peter H. Given
Coal Research Section
College of Earth and Mineral Sciences
The Pennsylvania State University
University Park, PA 16802

ABSTRACT

In an effort to understand the effect of oxidation of coal on the composition of liquefaction products, a sample of hvAb coal from the Lower Kittanning Seam in Pennsylvania, labelled PSOC-1336, was oxidized in the presence of air in a convection oven at 140°C for 16 days and liquefied in tubing bomb reactors in the presence of tetralin. The oxidation of coal decreased the liquefaction conversion. The aromatic fraction of the hexane-soluble oil from oxidized coal contained smaller amounts of phenanthrenes and pyrenes and larger amounts of tetralin-related artifacts when compared to that from the fresh coal. Relatively larger amounts of the hydroxy derivatives of indane, naphthalene, fluorene and phenanthrene were present in the polar fraction from the oxidized coal.

INTRODUCTION

It is known that coals deteriorate on oxidation and the extent of deterioration depends on the severity of oxidation conditions. The earliest study on the mechanism of oxidation of coals was reported by Jones and Townend in 1945 (1). After a lack of interest for more than two decades, there has been renewed interest in studying the effect of oxidation on the physical and chemical characteristics of coals (2,3). New analytical techniques to detect oxidation (4,5) and the mechanism and kinetics of oxidation have been reported (6,7). Few studies exist on the effects of partial oxidation on the liquefaction behavior of coals (8-10).

EXPERIMENTAL

The objective of this study is to understand the effects of oxidation on the liquefaction behavior of coals and on the composition of liquefaction products. A sample of hvAb coal from the Lower Kittanning seam in Pennsylvania (PSOC-1336) was oxidized by exposure to air in an oven at 140°C for 16 days and then liquefied in tubing bomb reactors using tetralin as donor vehicle under fairly mild conditions (400°C, one hour, no hydrogen gas). The unoxidized coal was also liquefied under identical conditions for comparison.

Present address: Process Sciences Division, Department of Applied Science, Brookhaven National Laboratory, Upton, New York 11973

RESULTS AND DISCUSSION

The characteristics of the coal are given in Table 1 and the basic liquefaction data are shown in Table 2. The total conversion into ethyl acetate-soluble products plus gases was slightly higher in the case of the unoxidized coal. The higher conversion was reflected in a higher yield of liquid products whereas yield of gases actually decreased. This shows that oxidation is detrimental to coal liquefaction. Similar results have been reported (9,10).

The hexane-soluble oil was vacuum distilled at 70°C (about 2 mm Hg pressure) to remove naphthalene and excess tetralin as completely as possible. A primary fractionation of the oil into saturate, aromatic and polar fractions was made by HPLC (Waters Associates) using a semi-preparative micro-Bondapak NH_2 column. Table 2 does not show appreciable differences with respect to the yield of individual fractions.

All fractions were analyzed by capillary-GC/MS (Finnigan 4000) using a 30 meter SE-54 column to obtain product composition data. The n-alkane distribution in the saturate fraction of the oil from unoxidized coal is compared with that of the oxidized coal in Figure 1. The differences are minor with respect to the modality of distribution as well as the yield of individual hydrocarbons. However, GC/MS characterization of the aromatic fractions revealed important differences.

Figure 2 shows the gas chromatograms of aromatic fractions and the peaks are identified in Table 3. The aromatic fractions contained various dimeric artefacts (hydrogenated binaphthyls) formed from the tetralin donor vehicle during coal liquefaction. Pyrites and clay minerals were found to independently catalyze these reactions (11). Table 4 shows that the yield of selected artifacts, binaphthyl, tetrahydro-, and octahydro-binaphthyl, were much higher when the coal was oxidized.

It is known that exposure of coals to air at temperatures below 80°C, leads to the formation of peroxides (1). These unstable species may be transient intermediates at somewhat higher temperatures, leading to the formation of various oxygen functions, notably carbonyl. Carbonyl is easily reduced if a supply of hydrogen is available, and so will tend to promote both generation of free radicals from the solvent and increased consumption of it. This, perhaps, is the chief factor responsible for the production of dimers from the solvent. Additionally, the oxidation would have converted the pyrite present in the coal (2.1% dmmf) to sulfates and sulfuric acid, which might have influenced the dimerization. In any case, an enhancement in the production of artefacts could limit the availability of hydrogen from the donor solvent which, in turn, can affect the yield of smaller molecules that are formed via hydrocracking and there are obvious implications for recycle solvent quality and consumption.

Benzylic CH_2 groups in diaryl-methanes and diaryl-ethanes are likely to be particularly susceptible for oxidation. Once oxidized, they can no longer cleave to methyl-substituted aromatic structrues. Thus, one might expect methyl substitution to be reduced in the liquefaction products of an oxidized coal. The product yield data in Table 4 for some selected polynuclear aromatic hydrocarbons, lend support to this argument, though they cannot be said to prove it.

The differences in composition of the polar fraction are considerably larger. The oxidized coal afforded a richer, more complex mixture of compounds and structural types than the unoxidized (Figure 3 and Table 5). At the lower end of the molecular weight range, there are large numbers of alkyl-hydroxy-benzenes and alkyl-indanols. The fractions from both oxidized and unoxidized coals showed a number of alkyl-hydroxy-naphthalenes, but in the higher end of the molecular weight range, hydroxy-fluorene and hydroxy-phenanthrenes were more abundant and richer in the polar fractions from the oxidized sample.

A comparison of the FTIR spectra of oxidized and unoxidized coals showed the expected increase due to carbonyl group absorption (1690 cm^{-1}), but also showed an increase of singly-bonded oxygen (ether or phenolic). Reduction of carbonyl and cleavage of ethers, as well as direct insertion of OH, could all contribute to a more complex mixture of phenols in the liquefaction product of an oxidized coal.

CONCLUSIONS

The laboratory low-temperature oxidation of a coking Pennyslvania coal, PSOC-1336, decreases the liquefaction conversion into ethylacetate solubles plus gases. The ratio of dimeric solvent artefacts to coal products was much greater in hexane-soluble oil from the oxidized sample. An enhancement in the yield of solvent artefacts could indirectly affect the yield of smaller molecules that are formed via cracking. The liquefaction products of the oxidized coal contained less methyl substitution but larger amounts of hydroxy derivatives of indane, naphthalene, fluorene and phenanthrene.

ACKNOWLEDGEMENTS

This work was supported by the U.S. Department of Energy, Contract No. EX-76-C-01-2494 and the coal used in this study was drawn from the Penn State/DOE Coal Sample and Data Base.

REFERENCES

1. Jones, R. E., and Townend, D. T. A., Nature, 155, 424 (1945).
2. Rhoads, C. A., Senftle, J. T., Coleman, M. M., Davis, A., and Painter, P. C. Fuel, 62, 1387 (1983).
3. Cronauer, D. C., Ruberto, R. G., Jenkins, R. J., Davis, A., Painter, P. C., Hoover, D. S., Strasinic, M. E., and Schlyer, D., Fuel, 62, 1127 (1983).
4. Gray, R. J., Rhodas, A. H., and King, D. T., Soc. Mining Engineers, Trans., 260(4), 334 (1976).
5. Painter, P. C., Snyder, R. W., and Kwong, J., Fuel, 59, 282 (1980).
6. Marinov, V. N., Fuel, 56, 158 (1977).
7. Cronauer, D. C., Ruberto, R. G., Silver, R. S., Jenkins, R. J., Ismail, I. M. K., Schlyer, D., Fuel, 62, 1117 (1983).
8. Cronauer, D. C., Ruberto, R. G., Silver, R. S., Jenkins, R. J., and Davis, A. EPRI Report No. AP-1625, Project 779-25, EPRI, Palo Alto, CA., 1980.
9. Whitehurst, D. D., Mitchell, T. O., and Farcasiu, M., "Coal Liquefaction: The Chemistry and TEchnology of Thermal Processing", Academic Press, NY., 1980.
10. Neavel, R. C., Fuel, 55, 237 (1976).
11. Sundaram, M. S., and Given, P. H., ACS Div. Fuel Chem., Prepr. 28(5), 26 (1983).

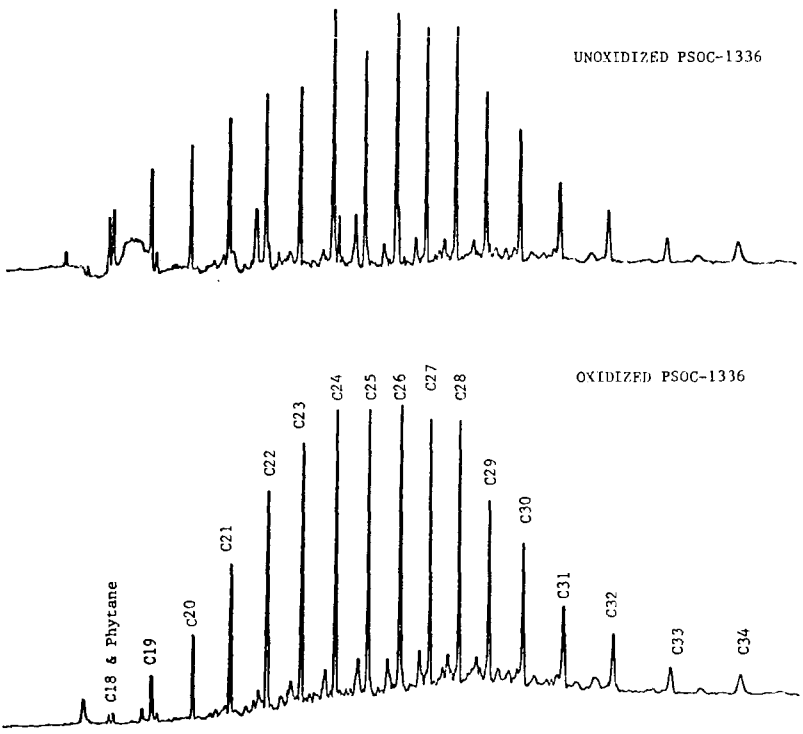

FIGURE 1. TOTAL ION CHROMATOGRAM OF SATURATED FRACTIONS

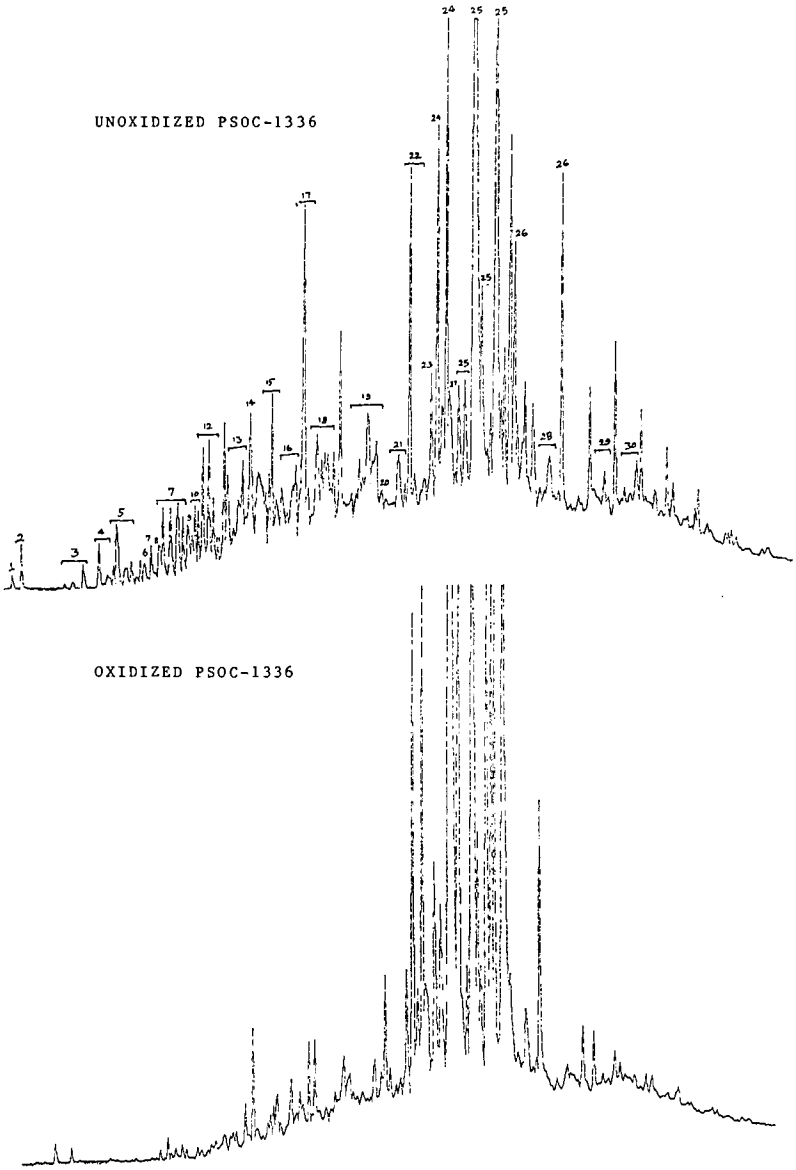

FIGURE 2. TOTAL ION CHROMATOGRAM OF AROMATIC FRACTIONS

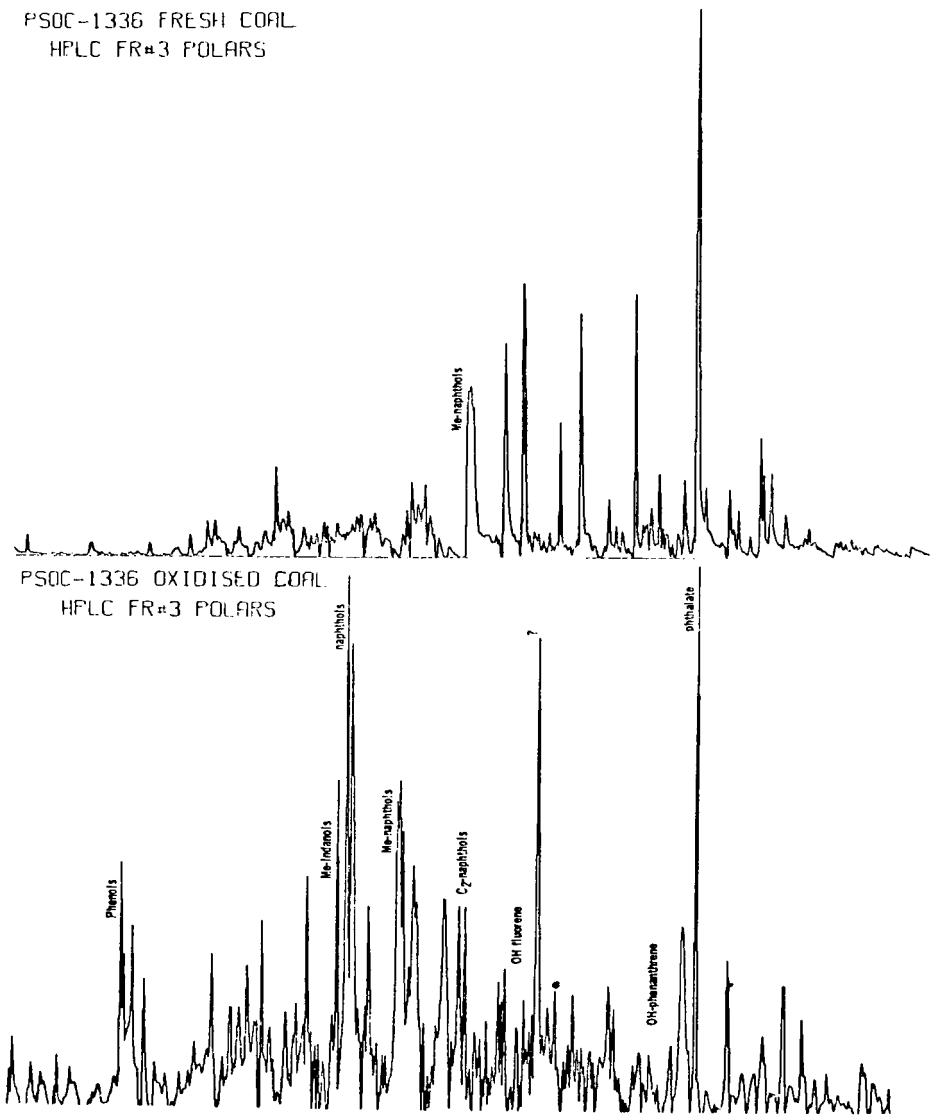

FIGURE 3. TOTAL ION CHROMATOGRAM OF POLAR FRACTIONS

TABLE 1

Analytical Data for PSOC-1336, Lower Kittannning Seam, Pa.

dry mineral matter free			
C	87.2%	vitrinite	85%
H	5.4	liptinites	5%
N	1.6	inertinite	10%
S	1.0	dry basis:	
Cl	0.1	mineral matter	16.7% (including pyrite 2.1%)
O(diff)	4.6		

ASTM rank class: hvAb

TABLE 2

Liquefaction Data

	Unoxidized	Oxidized
Product Yields:(%dmmf coal)		
Asphaltenes	19.9	14.9
Oil	11.0	7.2
Gases	3.3	7.2
Conversion	34.2	29.3
Oil Composition:(% oil)		
Saturates	2.8	2.6
Aromatics	42.3	40.0
Polars	54.9	57.4

TABLE 3

Identification of Aromatic Hydrocarbons

Peak Number	Identification
1	Tetralin
2	Naphthalene
3	Methylnaphthalene
4	Tetrahydromethylnaphthalene
5	C_2-Naphthalene
6	Acenaphthene
7	C_3-Naphthalene
8	C_1-Acenaphthene
9	Fluorene
10	C_1-Biphenyl
11	C_2-Acenaphthene
12	C_1-Dibenzofuran + C_4-Naphthalene
13	C_2-Dibenzofuran/C_2-Biphenyl
14	Phenanthrene
15	C_3-Biphenyl
16	C_4-Biphenyl
17	C_1-Phenanthrene
18	C_2-Phenanthrene
19	Fluoranthene/C_3-Phenanthrene
20	Pyrene
21	C_3-Phenantherene
22	C_1-Pyrene
23	Benzofluorene
24	Tetrahydrobinaphthyl
25	Octahydrobinaphthyl
26	Binaphthyl
27	Chrysene/Triphenylene/ Benzanthracene, Methyl
28	Benzofluoranthene
29	Benzopyrene/Perylene
30	Benzopyrene/Perylene, Methyl

TABLE 4

Yields of Selected Components in the Aromatic Fraction of PSOC-1336

	Unoxidized	Oxidized
Artefacts (ug/gm oil)		
Binaphthyl	73	290
Tetrahydrobinaphthyl	103	336
Octahydrobinaphthyl	211	348
Total artefacts	387	973
Coal-derived (in ug/gm dry coal)		
Phenanthrene	3.3	1.8
C_1-Phenanthrenes	11.3	5.6
C_2-Phenanthrenes	18.1	8.8
Pyrene	3.0	2.5
C_1-Pyrenes	23.7	16.5
C_2-Pyrenes	25.3	20.4
C_3-Pyrenes	8.1	5.0
Benzopyrene and its isomers	28.5	26.8

TABLE 5

Compounds identified in the Polar Fraction *

Phenol	Naphthol
Methylphenol	Methylnaphthol
C_2-Phenol	C_5-Phenol
C_3-Phenol	C_2-Naphthol
Indole	Hydroxyfluorene
Indanol	C_1-Dibenzofuran
Dihydroxybenzene	Xanthene
C_4-Phenol	C_1-Hydroxyfluorene
Indenol	C_2-Hydroxyfluorene
Methylindanol	Hydroxyphenanthrene
Methylindole	Diisobutylphthalate (impurity)
C_2-Indanols	
Phenylfuran	

* From Oxidized Coal